

Geophysical Research Letters®



RESEARCH LETTER

10.1029/2023GL107990

Key Points:

- Associative detachment of electrons in sprites proceeds almost exclusively from vibrationally excited N₂
- We provide updated rate coefficients for electron associative detachment
- In models with the updated rates, sprite glows persist tens of milliseconds, in agreement with observations

Supporting Information:

Supporting Information may be found in the online version of this article.

Correspondence to:

A. Malagón-Romero and A. Luque,
malagon@cwi.nl;
luque@iaa.es



Citation:

Malagón-Romero, A., Luque, A., Shuman, N. S., Miller, T. M., Ard, S. G., & Viggiano, A. A. (2024). Associative electron detachment in sprites. *Geophysical Research Letters*, 51, e2023GL107990. <https://doi.org/10.1029/2023GL107990>

Received 22 DEC 2023

Accepted 29 MAY 2024

Associative Electron Detachment in Sprites

A. Malagón-Romero^{1,2} , A. Luque¹ , Nicholas S. Shuman³, Thomas M. Miller⁴, Shaun G. Ard³, and Albert A. Viggiano³

¹Instituto de Astrofísica de Andalucía (IAA), CSIC, Granada, Spain, ²Centrum Wiskunde and Informatica (CWI), Amsterdam, The Netherlands, ³Air Force Research Laboratory, Space Vehicles Directorate, Kirtland AFB, Albuquerque, NM, USA, ⁴Boston College Institute for Scientific Research, Boston, MA, USA

Abstract The balance of processes affecting electron density drives the dynamics of upper-atmospheric electrical events, such as sprites. We examine the detachment of electrons from negatively charged atomic oxygen (O⁻) via collisions with neutral molecular nitrogen (N₂) leading to the formation of nitrous oxide (N₂O). Past research posited that this process, even without significant vibrational excitation of N₂, strongly impacts the dynamics of sprites. We introduce updated rate coefficients derived from recent experimental measurements which suggest a negligible influence of this reaction on sprite dynamics. Given that previous rates were incompatible with the observed decay of the light emissions from sprite glows, our findings support that glows actually result from electron depletion in sprite columns.

Plain Language Summary Sprites are transient, filamentary luminous structures appearing between approximately 50 and 85 km above Earth's surface. While the primary sprite activity is ephemeral, lasting mere thousandths of a second, certain luminous features persist up to a hundred times longer. The key to understanding these enduring structures lies in the evolution of free electron populations that facilitate electrical conductivity. Here we show that a process that influences this population is slower than previously thought. This may explain why luminous structures can persist for so long.

1. Introduction

Sprites are high-altitude filamentary discharges occurring in the upper mesosphere following a strong cloud-to-ground lightning discharge in a thunderstorm (Liu et al., 2015; Luque & Ebert, 2009; Pasko et al., 1997). One notable benefit arising from the discovery of sprites (Franz et al., 1990) has been a renewed interest in the chemistry of the upper mesosphere, in particular on the reaction mechanisms induced by free, super-thermal electrons as present in sprites, where they are accelerated by intense electric fields. Several questions motivate this interest: for example, there is the question of whether sprites have global, regional, or local effects on the composition of the atmosphere (Arnone et al., 2008; Gordillo-Vázquez & Pérez-Invernón, 2021; Malagón-Romero et al., 2023; Sentman et al., 2008). Understanding the spectra of sprites (Gordillo-Vázquez et al., 2012; Passas et al., 2016) is another motivation, particularly relevant in the context of space-based detection of sprites (Chanrion et al., 2019) and discrimination from other events such as Blue Luminous Events (BLUEs) in thundercloud tops (Chanrion et al., 2017; Soler et al., 2020).

Finally, understanding the chemistry of electrons and ions in the upper mesosphere is crucial for elucidating the fundamental physics of sprites. Conversely, investigations into sprites have highlighted previously overlooked reactions. A notable example is the reaction of detachment of electrons from O⁻ to form N₂O, which is the focus of the present work:



Several numerical modeling works (Kotovskiy & Moore, 2017; Liu, 2012; Luque & Gordillo-Vázquez, 2012; Neubert & Chanrion, 2013) highlighted the prominent role of the detachment reaction from O⁻ on the sprite inception and dynamics. In sub-breakdown electric fields, the free electron population is not solely determined by ionization reactions and their counterpart, attachment reactions, but also by detachment reactions such as Equation 1 that reverse this attachment and return electrons to their free state. All these works assumed the most recent laboratory measurements of reaction Equation 1 provided by Rayment and Moruzzi (1978), who argued that the reaction is effective even when nitrogen is in its vibrational ground state. The detachment rates by

© 2024. The Author(s).

This is an open access article under the terms of the [Creative Commons Attribution-NonCommercial-NoDerivs License](#), which permits use and distribution in any medium, provided the original work is properly cited, the use is non-commercial and no modifications or adaptations are made.

Rayment and Moruzzi (1978) have been used in different contexts besides sprites. For instance, Pan-cheshnyi (2013) considered how, among others, reaction Equation 1 influences an effective ionization rate whereas da Silva and Pasko (2013) applied them to their investigation of the streamer-to-leader transition.

Other investigations, such as Luque et al. (2016) indicated potential inaccuracies in the reaction rate coefficients of Rayment and Moruzzi (1978). That study explained the appearance in sprites of beads and glows, which are luminous structures that persist for up to 100 milliseconds even after the main streamer activity has subsided (Stenbaek-Nielsen & McHarg, 2008). The model presented by Luque et al. (2016) matched the observed sprite glow lifetimes as long as detachment reactions such as Equation 1 were disregarded. This was later confirmed by Malagón-Romero et al. (2020), where a similar mechanism was proposed as the origin of upward branches in sprites which frequently, if not always, emerge from pre-existing glows.

A further step was taken in a careful literature analysis by Janalizadeh and Pasko (2021), where, besides identifying several issues in the data reporting by Rayment and Moruzzi (1978), they pointed that under atmospheric conditions electron detachment from O^- is not possible in collisions with nitrogen in its ground state.

The controversy motivated Shuman et al. (2023-a) to carry out new measurements of the reaction rate of Equation 1. The rate coefficients of $O^- + N_2$ were measured using a flow tube apparatus under thermal conditions from 800 to 1200 K; at lower temperatures the rate coefficients were smaller than the limit of the experiment. The results were inconsistent with the literature determination by Rayment and Moruzzi (1978), but supported the results of Janalizadeh and Pasko (2021) indicating that reaction with vibrational ground state N_2 was negligible. The results were model fitted and vibrationally resolved rate constants for $v \leq 2$ derived with extrapolation over the thermal range 300–1,400 K.

The objective of this study is to investigate the implications of an enhanced understanding of reaction Equation 1 on the chemistry of sprites and related high-atmosphere electrical phenomena. We hope that this work will garner interest of the geophysical community into the updated knowledge of electron detachment in the atmosphere.

2. Updated Reaction Rate

As described in detail by Shuman et al. (2023-a), the $O^- + N_2$ associative detachment reaction must overcome two kinetic bottlenecks. First, a large energetic barrier separates the weakly bound entrance complex $O^-(N_2)$ from the metastable, but longer-lived, N_2O^- intermediate. Second, the system must cross from the N_2O^- anion potential surface to the N_2O neutral potential surface. It happens that both the height of the energetic barrier and the location of the lowest-energy crossing geometry are very similar, about 0.3 eV above the energy of the separated reactants. Shuman et al. (2023-a) successfully reproduced the measured thermal rate constants with a simple model, by considering only the vibrational state of N_2 and the relative kinetic energy of the reactants. Increased vibrational energy increased the probability of overcoming the transition state to N_2O^- (both from the inherently higher energy and from increased overlap with the geometry of the transition state, which lies at a larger N-N bond distance). Increased kinetic energy also increased the probability of overcoming the transition state, but decreased the probability of crossing to the neutral surface, such that increasing kinetic energy initially increases the rate coefficient but at larger values decreases the rate coefficient.

The vibrationally-resolved thermal rate constants reported by Shuman et al. (2023-a) can be converted to a function of E/n . The effective kinetic energy in the center-of-mass reference frame is given by the Wannier expression (Viggiano & Morris, 1996; Viggiano & Williams, 2001) and for our particular case reads:

$$\frac{3}{2}kT_{\text{eff}} = \frac{3}{2}kT_0 + \frac{1}{2}m_{N_2}v_d^2, \quad (2)$$

where k is the Boltzmann constant, T_{eff} is an effective translational temperature, T_0 is the gas temperature, m_{N_2} is the mass of the molecular nitrogen and v_d is the ion drift velocity. The drift velocity is a function of the applied electric field strength (E) divided by the air density (n) and the reduced ion mobility (κ_0)

$$v_d = \kappa_0 n_0 \frac{E}{n}, \quad (3)$$

Table 1

Reaction Rate Coefficients for the Reaction $O^- + N_2(\nu) \rightarrow N_2O + e$ for Different Values of an Effective Collision Temperature T_{eff} and Reduced Electric Field E/n

T_{eff} (K)	E/n (Td)	K_0 ($\text{m}^2 \text{V}^{-1} \text{s}^{-1}$)	k ($\text{m}^3 \text{s}^{-1}$)		
			$\nu = 0$	$\nu = 1$	$\nu = 2$
200	0	3.33×10^{-4}	2.33×10^{-26}	5.42×10^{-19}	1.72×10^{-17}
300	32	3.5×10^{-4}	1.06×10^{-23}	9.93×10^{-19}	1.42×10^{-17}
400	43	3.67×10^{-4}	2.23×10^{-22}	1.29×10^{-18}	1.22×10^{-17}
500	50	3.81×10^{-4}	1.34×10^{-21}	1.47×10^{-18}	1.06×10^{-17}
600	56	3.94×10^{-4}	4.56×10^{-21}	1.57×10^{-18}	9.42×10^{-18}
700	61	4.06×10^{-4}	1.07×10^{-20}	1.63×10^{-18}	8.43×10^{-18}
800	65	4.17×10^{-4}	2.02×10^{-20}	1.66×10^{-18}	7.60×10^{-18}
900	69	4.27×10^{-4}	3.30×10^{-20}	1.67×10^{-18}	6.90×10^{-18}
1,000	72	4.35×10^{-4}	4.85×10^{-20}	1.67×10^{-18}	6.30×10^{-18}
1,100	75	4.43×10^{-4}	6.62×10^{-20}	1.65×10^{-18}	5.78×10^{-18}
1,200	78	4.5×10^{-4}	8.56×10^{-20}	1.63×10^{-18}	5.32×10^{-18}
1,300	81	4.55×10^{-4}	1.06×10^{-19}	1.60×10^{-18}	4.91×10^{-18}
1,400	83	4.56×10^{-4}	1.26×10^{-19}	1.56×10^{-18}	4.55×10^{-18}
1,500	86	4.59×10^{-4}	1.46×10^{-19}	1.53×10^{-18}	4.23×10^{-18}
1,600	89	4.62×10^{-4}	1.66×10^{-19}	1.49×10^{-18}	3.94×10^{-18}
1,700	91	4.66×10^{-4}	1.85×10^{-19}	1.45×10^{-18}	3.67×10^{-18}
1,800	94	4.69×10^{-4}	2.03×10^{-19}	1.45×10^{-18}	3.43×10^{-18}
1,900	96	4.72×10^{-4}	2.19×10^{-19}	1.36×10^{-18}	3.21×10^{-18}
2,000	99	4.75×10^{-4}	2.34×10^{-19}	1.32×10^{-18}	3.01×10^{-18}
2,100	102	4.78×10^{-4}	2.48×10^{-19}	1.28×10^{-18}	2.83×10^{-18}
2,200	105	4.8×10^{-4}	2.60×10^{-19}	1.24×10^{-18}	2.66×10^{-18}
2,300	107	4.83×10^{-4}	2.71×10^{-19}	1.20×10^{-18}	2.50×10^{-18}
2,400	110	4.85×10^{-4}	2.80×10^{-19}	1.16×10^{-18}	2.36×10^{-18}
2,500	113	4.87×10^{-4}	2.89×10^{-19}	1.12×10^{-18}	2.23×10^{-18}
2,600	117	4.89×10^{-4}	2.95×10^{-19}	1.08×10^{-18}	2.11×10^{-18}
2,700	120	4.91×10^{-4}	3.01×10^{-19}	1.04×10^{-18}	1.99×10^{-18}
2,800	123	4.93×10^{-4}	3.06×10^{-19}	1.01×10^{-18}	1.89×10^{-18}
2,900	127	4.95×10^{-4}	3.09×10^{-19}	9.77×10^{-19}	1.79×10^{-18}
3,000	131	4.97×10^{-4}	3.12×10^{-19}	9.44×10^{-19}	1.70×10^{-18}

Note. K_0 is the mobility of O^- ions for the given electric field, at atmospheric pressure and 300 K. For drift velocities below 10^3 ms^{-1} (reduced electric fields below $E/n \approx 85 \text{ Td}$) we use ion mobilities interpolated from Viehland and Mason (1995) for higher reduced electric fields we extrapolate as $K_0 = 1 \times 10^{-4} \text{ m}^2 \text{V}^{-1} \text{s}^{-1} \times \ln(v_d(T_{\text{eff}})/10^{-2} \text{ m s}^{-1}) - 7 \times 10^{-4} \text{ m}^2 \text{V}^{-1} \text{s}^{-1}$.

where n_0 is Loschmidt's number. We can then define the drift velocity at temperature T_0 equivalent to the thermal velocity at temperature T_{eff} as

$$v_d(T_{\text{eff}}, T_0) = \left[\frac{3k(T_{\text{eff}} - T_0)}{m_{N_2}} \right]^{1/2}. \quad (4)$$

Here T_0 is taken to be 200 K, an approximation for the gas temperature at an altitude of 70 km and T_{eff} are the temperatures reported by Shuman et al. (2023-a). The values of κ_0 are interpolated from the compilation of Viehland and Mason (1995) up to $E/n = 100 \text{ Td}$ and extrapolated from that data up to 120 Td. Table 1 contains the resulting reaction rate coefficients for reaction Equation 1.

Table 2
Fitting Parameters for the Reaction Rate Coefficients for the Reaction $O^- + N_2(v) \rightarrow N_2O + e$ With $v = 0, 1, 2$ According to Expression 5

v	k_0 ($m^3 s^{-1}$)	T_A (K)	d	E_A/n (Td)
0	3.98×10^{-17}	5,097	-1.36	176
1	9.04×10^{-18}	674	-0.85	64
2	2.74×10^{-17}	186	-1.10	34

The dependence of the reaction rate coefficients on the effective temperature is well approximated by a modified Arrhenius expression of the form

$$k = k_0 \left(\frac{T_{\text{eff}}}{300 \text{ K}} \right)^d \exp \left(-\frac{T_A}{T_{\text{eff}}} \right). \quad (5)$$

The best-fit parameters k_0 , T_A and d for $v = 0, 1, 2$ are listed in Table 2. Figure 1 shows the rate coefficients as well as the values from expression Equation 5. Also, as a reasonable approximation that foregoes the use of

interpolating tables for the ion mobility, we also show the results of Equation 5 with a constant reduced ion mobility $\kappa_0 = 4.5 \times 10^{-4} m^2 V^{-1} s^{-1}$. By further neglecting T_0 in 4, we reach this simple expression for the reaction rate coefficient:

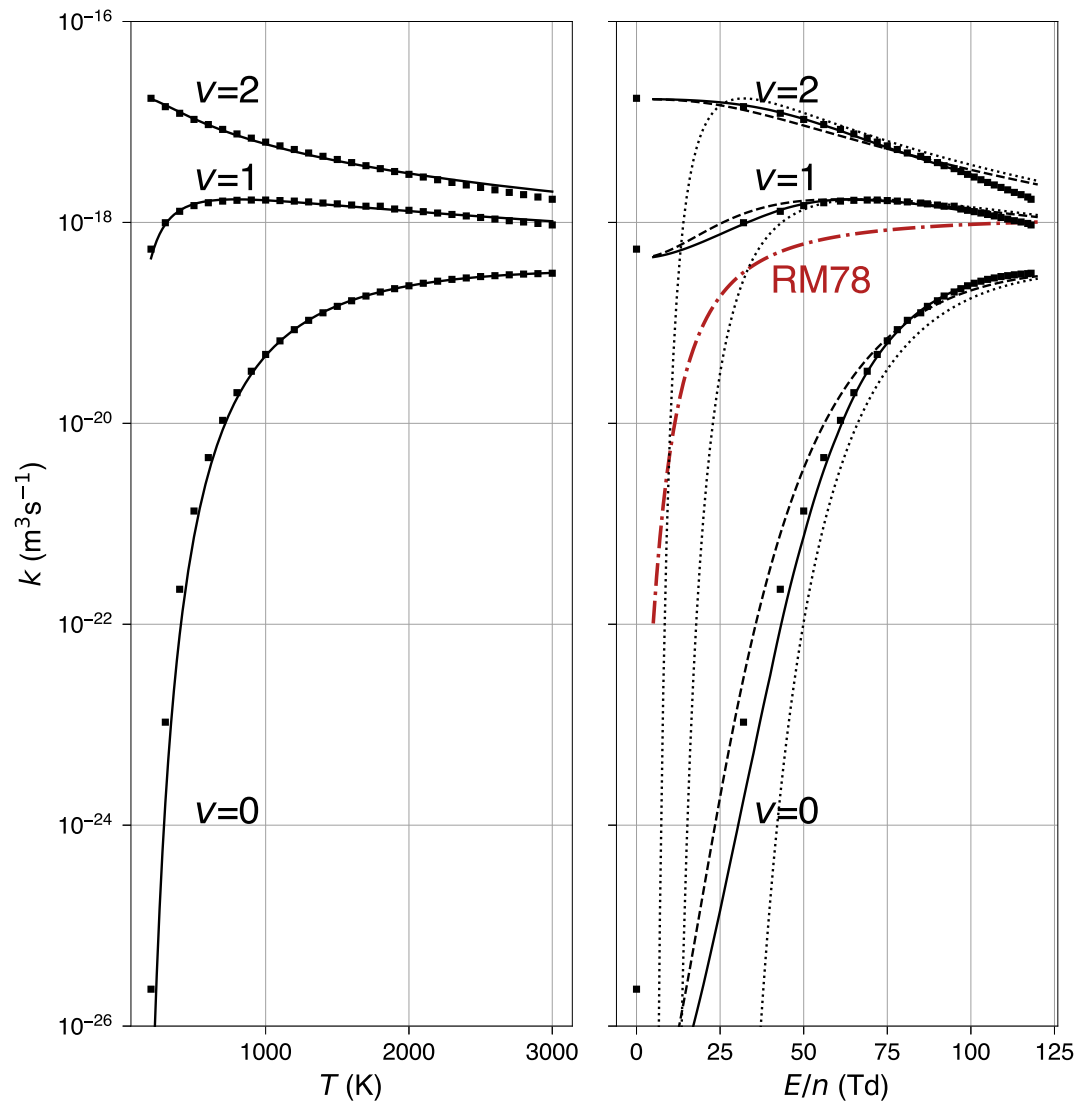


Figure 1. Rate coefficients of $O^- + N_2(v) \rightarrow N_2O + e$ for $v = 0, 1, 2$. On the left panel we show the dependence of the rate coefficients on temperature assuming equilibrium conditions. The dots correspond to the values in Table 1 whereas lines show the fits using Equation 5 with the parameters listed in Table 2. The right panel shows the rate dependence on the reduced electric field, following the conversion of Equations 3 and 4 with $T_0 = 200$ K. The solid lines use the same fits as in the left panel and the ion mobilities from Viehland and Mason (1995). The dashed lines replace these mobilities by a field-independent reduced ion mobility $\kappa_0 = 4.5 \times 10^{-4} m^2 V^{-1} s^{-1}$ and the dotted lines also neglect thermal motion ($T_0 = 0$).

$$k = k_0 \left(\frac{E/n}{43 \text{ Td}} \right)^{2d} \exp \left(- \left(\frac{E_A/n}{E/n} \right)^2 \right), \quad (6)$$

with the values of reduced electric fields E_A/n listed in the last column of Table 2. These rate coefficients are represented in 1 with dotted lines; they provide a reasonable approximation for reduced electric fields above 40 Td, where the energy imparted by the electric field dominates over thermal motion at 200 K.

We also plot in Figure 1 the reaction rate coefficients by Rayment and Moruzzi (1978) as approximated by Pancheshnyi (2013) (labeled as RM78). For most of the studied range of reduced electric field, the updated rate coefficients for the vibrational ground state of N_2 ($v = 0$) are several orders of magnitude below those from Rayment and Moruzzi (1978). Close to the classical breakdown field ($E/n \approx 120$), the updated rate is still about five times lower than RM78.

3. Implications

We now discuss some of the implications of the new rates on the physics of upper-atmospheric electrical discharges. Table S1 in the Supporting Information S1 details a simple chemical scheme that accounts for the main processes within a halo or sprite discharge and up to about 100 ms after its initiation. The rate coefficients for electron-molecule processes, which depend on the electron energy distribution function, are modeled by solving the steady-state Boltzmann equation with the Bolsig + solver (Hagelaar & Pitchford, 2005) and the Phelps' cross-section database (Lawton & Phelps, 1978; Phelps & Pitchford, 1985) as provided by LxCat (Carbone et al., 2021; Pancheshnyi et al., 2012; Pitchford et al., 2017). With these rates we approximate the vibrational distribution of the electronic ground state of nitrogen, which induce associative detachment from O^- with the rates discussed in the previous section. We also consider detachment from O_2^- and negative ion conversion as modeled by Pancheshnyi (2013). Finally, for the sake of completeness, we include positive ion conversion as modeled by Aleksandrov and Bazelyan (1999) and electron-ion and ion-ion recombination as modeled by Kossyi et al. (1992).

To compare with previous models, we also consider a reaction scheme where the rate of Equation 1 follows Rayment and Moruzzi (1978) as fitted by Pancheshnyi (2013) and regardless of the vibrational state of N_2 . We name the two models “new” and “RM78.”

First we look at the chemical evolution under constant reduced electric field. Figure 2 shows the evolution of the main negatively-charged species in the wake of a streamer that leaves an electron density $n_e = 10^{11} \text{ m}^{-3}$ at an altitude of 80 km. The left column of the figure (labeled (a)) corresponds to the reaction rates of Equation 1 presented here, whereas the right column (b) contains the densities predicted by the rates by Rayment and Moruzzi (1978). In both cases we simulate constant applied reduced electric fields of 70 Td and 90 Td.

There are clear differences between the two columns. Enhanced detachment rates of O^- in the right column yields higher electron and O^- densities by the end of the simulated evolution. Electron densities with the updated and the RM78 rates start to diverge at around 1 ms. Specifically, at an electric field strength of 70 Td with the updated rate coefficients, the electron density exhibits a two-order-of-magnitude reduction prior to stabilization. In contrast, according to the rate coefficients of Rayment and Moruzzi (1978), the electron density experiences only a marginal decrease before entering a growth regime. At 90 Td, and considering the new updated rates, the reduction in the electron density is still a factor of 6 greater than the obtained with the rate coefficients by Rayment and Moruzzi (1978). The evolution of the vibrational populations considered in this model is represented in Figure S1 in the Supporting Information S1, where we see that, despite being populated by electron impact, the densities of the $v = 1$ and $v = 2$ states remain at least two orders of magnitude below the density of the vibrational ground state.

Next we investigate the consequences of the updated reaction rate coefficient in a self-consistent 2D axisymmetric model of a sprite discharge. In this model, the electron density (n_e) under a local electric field E , evolves according to the conservation equation:

$$\partial_t n_e = \nabla \cdot (\mu_e E + D_e \nabla n_e) + C_e, \quad (7)$$

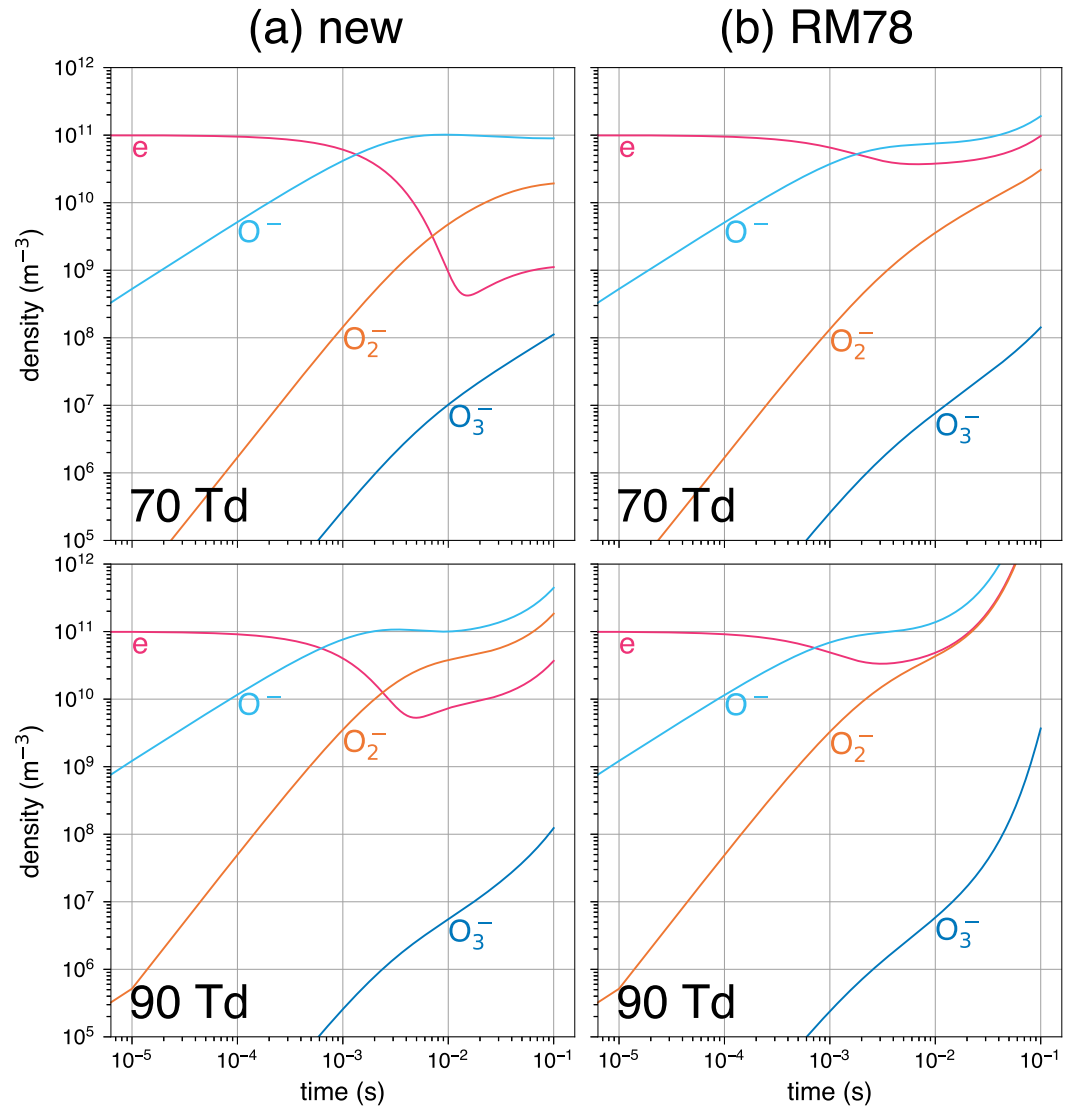


Figure 2. Evolution of the dominant negatively-charged species in our chemical models under a constant reduced electric field. Starting with an initial condition of an electron density of 10^{11} m^{-3} , which is representative of the state of a sprite column in the wake of a streamer at 80 km.

where μ_e and D_e are the electron mobility and the diffusion coefficient, and C_e is the chemical source term accounting for the chemical reactions listed in Table S1 in the Supporting Information S1. Transport coefficients (μ_e and D_e) are assumed to be functions of the local electric field and are computed with Bolsig+ (Hagelaar & Pitchford, 2005) using as above the cross sections for electron impact with N_2 and O_2 provided in Phelps' database retrieved from LxCat.

Neutral species and ions (n_i with $i = 0, 1, \dots$) are considered motionless and their time evolution obeys a simplified version of Equation 7, namely,

$$\partial_t n_i = C_i, \quad (8)$$

where C_i is the chemical source term determined by the reactions in Table S1 in the Supporting Information S1.

The electric field \mathbf{E} , is calculated as $\mathbf{E} = -\nabla\phi$, where ϕ is the electrostatic potential obtained upon the solution of Poisson's equation

$$\nabla^2 \phi = \sum_s \frac{q_s n_s}{\epsilon_0}, \quad (9)$$

where the sum extends over all charged species s , q_s is the charge of the species s and ϵ_0 is the vacuum permittivity.

The model is implemented in Afivo-streamer (Teunissen & Ebert, 2017) and is based on Afivo (Teunissen & Ebert, 2018), an octree-based adaptive mesh refinement framework, with OpenMP capabilities and a geometric multigrid solver for Poisson's equation. Equations 7 and 8 are solved with an explicit second order time stepping and a flux-limited second order accurate spatial discretization.

In this study, we initiate our model with the exact same conditions discussed by Malagón-Romero et al. (2020), that consist in a neutral column of radius $a_0 = 400$ m with a truncated funnel attached to its lower part that roughly approximates the multiple branching events the parent streamer discharge undergoes as it propagates. The initial electron density is then computed as

$$n_e(r, z) = n_{e,0}(z) \frac{a_0^2}{a(z)} \max\left(0, 1 - \frac{r^2}{a(z)^2}\right) + n_{e,bg}(z), \quad (10)$$

where $n_{e,0}(z) = C n_{air}(z)$ is the electron density at the axis, $C = 3.33 \times 10^{-11}$, n_{air} is the air density obtained by scaling the ground air density $n_{air,0} = 2.5 \times 10^{25} \text{ m}^{-3}$ as $n_{air}(z) = n_{air,0} \exp(-z/7.2 \text{ km})$, and $a(z)$ is a piece-wise linear function that models the radius of the channel and the funnel, ensuring a smooth transition. The funnel has a radius of 5 km at the base $z_b = 50$ km with the upper vertex at $z_u = 60$ km and is calculated as

$$a(z) = \max\left(a_0, \frac{z_u - z}{z_u - z_b} \times 5 \text{ km}\right). \quad (11)$$

Finally, the background electron density follows the Wait-Spies profile estimated by Hu et al. (2007):

$$n_{e,bg}(z) = 10^{-2} \text{ cm}^{-3} \exp\left(\frac{z - 60 \text{ km}}{2.86 \text{ km}}\right). \quad (12)$$

The computational domain is a 10 km radius and 40 km height cylinder with its base at 40 km altitude. The minimum grid spacing in our simulation has been 1.22 m. We apply homogeneous Neumann boundary conditions at all boundaries to solve Equations 7 and 8. Poisson's equation has been solved with homogeneous Neumann boundary conditions at the outer radial boundary. The bottom boundary is grounded while the top boundary is set to a fixed voltage of 2.9 MV. The result is a constant background field of 72.38 V/m pointing downwards, setting a reduced electric field E/n_{air} of approximately 120 Td at roughly 77 km.

The results are displayed in Figure 3 where we show simulated light emissions (N2 1P) from the sprite column. With the detachment rate coefficients of Rayment and Moruzzi (1978) (RM78) a more elevated conductivity inside the column contributes to a fast screening of the electric field and light emissions that decay within a few milliseconds. On the other hand, with the updated rates of detachment (new), the attachment instability discussed for example, by Luque et al. (2016) leads to a sharply defined, light-emitting segment which is consistent with observations (Bór, 2013; Stenbaek-Nielsen & McHarg, 2008).

A closer look at the light-emitting segment in Figure 4 shows that the luminosity decays faster than exponentially within 5 ms when using the RM78 detachment rate coefficients. This contrasts with the results for the new detachment rate coefficients (Table 1). In this case, the luminosity exhibits an exponential decay, consistent with observations (Luque et al., 2016), with a decay constant of approximately 1.7 ms. The exponential trend becomes evident after 6 ms, whereas observations show it almost from the very beginning. We attribute this discrepancy to the neutral charge conditions used to initiate the simulation (Luque et al., 2016).

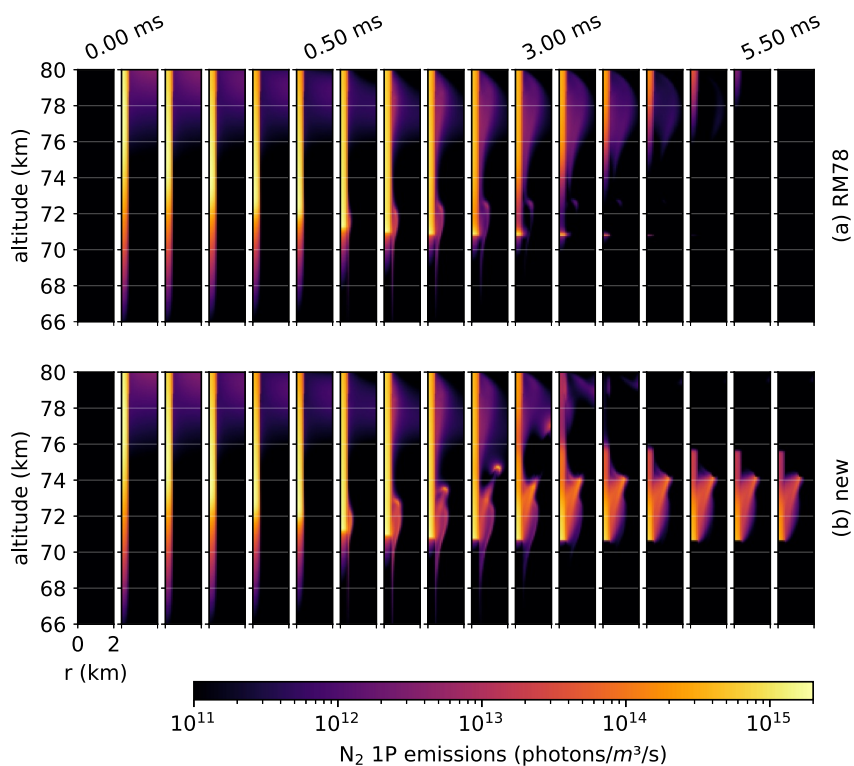


Figure 3. Modeled light emissions from a sprite column. Both for the reaction rate coefficients by Rayment and Moruzzi, (1978) (upper row) and the updated reaction rate coefficients in Table 1 (lower row), we show the instantaneous emissions of photons from the first positive system of molecular nitrogen (N_2 1P). The snapshots are taken at intervals of 0.1 ms up to 0.5 ms and of 0.5 ms afterward.

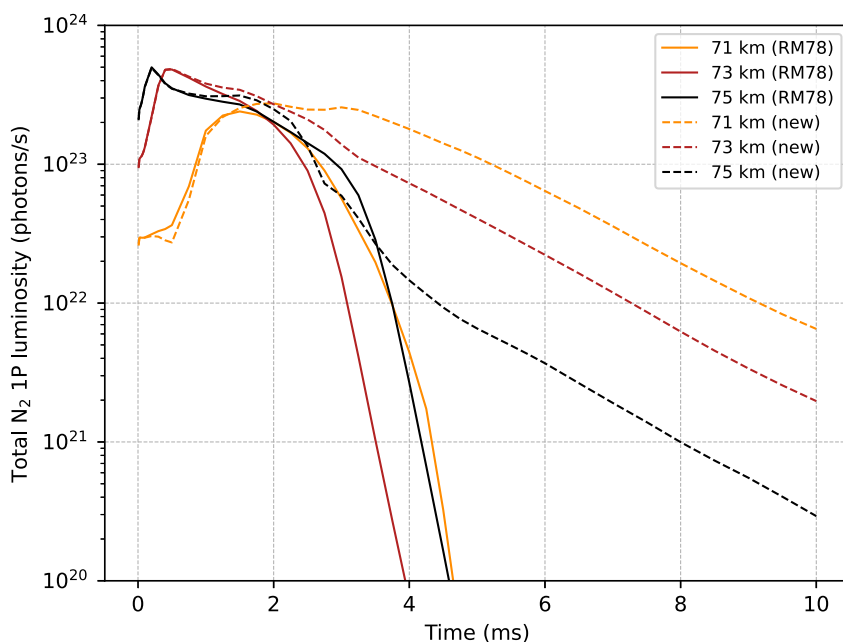


Figure 4. Emissions from the first positive system of N_2 integrated in 400 m-radius and 1 km-tall cylinders centered at 71 km, 73 and 75 km altitudes, considering the detachment rate coefficient from Rayment and Moruzzi (1978) (RM78) and the updated detachment rate coefficients from table 1 (new), showing faster than exponential and exponential decay respectively.

4. Conclusions

In this work we provide updated rate coefficients for the reaction of associative electron detachment and discuss its implications for the dynamics of sprites. For the vibrational ground state of N_2 , these rate are significantly smaller than previous estimates. We conclude that, given the low population of vibrationally excited N_2 , this reaction is too slow to play a significant role in sprites. Future investigations of electrical phenomena in the upper atmosphere should consider the new understanding of electron associative detachment presented here.

Data Availability Statement

The code containing the simple sprite chemical model used to generate Figure 2 is available in Malagón-Romero et al. (2024a). The output and source files for the generation of the results presented in Figures 3 and 4 are openly available in Malagón-Romero et al. (2024b).

Acknowledgments

A. Malagón-Romero and A. Luque acknowledge financial support from the Spanish Ministry of Science and Innovation, under project PID2022-136348NB-C31 and from the State Agency for Research of the Spanish MCIU through the “Center of Excellence Severo Ochoa” award for the Instituto de Astrofísica de Andalucía (CEX2021-001131-S). A. Malagón-Romero acknowledges the support from the grants BEVP34S12931 and BEVP34A6840 funded by “Ramón Areces Foundation.” The AFRL work is supported by the Air Force Office of Scientific Research for support under AFOSR-22RVCOR009. TMM is supported through the Institute for Scientific Research of Boston College under contract No. FA9453-20-C-0048. We thank Reza Janalizadeh for bringing the questions concerning the associative detachment to our attention. The views expressed are those of the authors and do not reflect the official guidance or position of the Department of the Air Force, the Department of Defense (DoD), or the United States government. The appearance of external hyperlinks does not constitute endorsement by the United States DoD of the linked websites, or the information, products, or services contained therein. The DoD does not exercise any editorial, security, or other control over the information you may find at these locations.

References

- Aleksandrov, N. L., & Bazelyan, E. M. (1999). Ionization processes in spark discharge plasmas. *Plasma Sources Science and Technology*, 8(2), 285–294. <https://doi.org/10.1088/0963-0252/8/2/309>
- Arnone, E., Kero, A., Dinelli, B. M., Enell, C. F., Arnold, N. F., Papandrea, E., et al. (2008). Seeking sprite-induced signatures in remotely sensed middle atmosphere NO_2 . *Geophysical Research Letters*, 35(5), L05807. <https://doi.org/10.1029/2007GL031791>
- Bór, J. (2013). Optically perceptible characteristics of sprites observed in Central Europe in 2007–2009. *Journal of Atmospheric and Solar-Terrestrial Physics*, 92, 151–177. <https://doi.org/10.1016/j.jastp.2012.10.008>
- Carbone, E., Graef, W., Hagelaar, G., Boer, D., Hopkins, M. M., Stephens, J. C., et al. (2021). Data needs for modeling low-temperature non-equilibrium plasmas: The LXC at project, history, perspectives and a tutorial. *Atoms*, 9(1), 16. <https://doi.org/10.3390/atoms9010016>
- Chanrion, O., Neubert, T., Lundgaard Rasmussen, I., Stoltze, C., Tcheriak, D., Jessen, N. C., et al. (2019). The modular multispectral imaging array (MMIA) of the ASIM payload on the international space station. *Space Science Reviews*, 215(4), 28. <https://doi.org/10.1007/s11214-019-0593-y>
- Chanrion, O., Neubert, T., Mogensen, A., Yair, Y., Stendel, M., Singh, R., & Siingh, D. (2017). Profuse activity of blue electrical discharges at the tops of thunderstorms. *Geophysical Research Letters*, 44(1), 496–503. <https://doi.org/10.1002/2016GL071311>
- da Silva, C. L., & Pasko, V. P. (2013). Dynamics of streamer-to-leader transition at reduced air densities and its implications for propagation of lightning leaders and gigantic jets. *Journal of Geophysical Research: Atmospheres*, 118(24), 13561–13590. <https://doi.org/10.1002/2013JD020618>
- Franz, R. C., Nemzek, R. J., & Winckler, J. R. (1990). Television image of a large upward electrical discharge above a thunderstorm system. *Science*, 249(4964), 48–51. <https://doi.org/10.1126/science.249.4964.48>
- Gordillo-Vázquez, F. J., Luque, A., & Simek, M. (2012). Near infrared and ultraviolet spectra of TLEs. *Journal of Geophysical Research: Space Physics*, 117(A5), A05329. <https://doi.org/10.1029/2012JA017516>
- Gordillo-Vázquez, F. J., & Pérez-Invernón, F. J. (2021). A review of the impact of transient luminous events on the atmospheric chemistry: Past, present, and future. *Atmospheric Research*, 252, 105432. <https://doi.org/10.1016/j.atmosres.2020.105432>
- Hagelaar, G. J. M., & Pitchford, L. C. (2005). Solving the Boltzmann equation to obtain electron transport coefficients and rate coefficients for fluid models. *Plasma Sources Science and Technology*, 14(4), 722–733. <https://doi.org/10.1088/0963-0252/14/4/011>
- Hu, W., Cummer, S. A., & Lyons, W. A. (2007). Testing sprite initiation theory using lightning measurements and modeled electromagnetic fields. *Journal of Geophysical Research: Atmospheres*, 112(D13), D13115. <https://doi.org/10.1029/2006JD007939>
- Janalizadeh, R., & Pasko, V. P. (2021). Implications of electron detachment in associative collisions of atomic oxygen anion with molecular nitrogen for modeling of transient luminous events. *Geophysical Research Letters*, 48(4), e91134. <https://doi.org/10.1029/2020GL091134>
- Kossyi, I. A., Kostinsky, A. Y., Matveyev, A. A., & Silakov, V. P. (1992). Kinetic scheme of the non-equilibrium discharge in nitrogen-oxygen mixtures. *Plasma Sources Science and Technology*, 1(3), 207–220. <https://doi.org/10.1088/0963-0252/1/3/011>
- Kotovsky, D. A., & Moore, R. C. (2017). Modeling long recovery early events (LOREs) produced by lightning-induced ionization of the nighttime upper mesosphere. *Journal of Geophysical Research: Space Physics*, 122(7), 7761–7780. <https://doi.org/10.1002/2017JA023996>
- Lawton, S. A., & Phelps, A. V. (1978). Excitation of the $b\ ^1\Sigma^+g$ state of O_2 by low energy electrons. *The Journal of Chemical Physics*, 69(3), 1055–1068. <https://doi.org/10.1063/1.436700>
- Liu, N. (2012). Multiple ion species fluid modeling of sprite halos and the role of electron detachment of O^- in their dynamics. *Journal of Geophysical Research: Space Physics*, 117(A3), A03308. <https://doi.org/10.1029/2011JA017062>
- Liu, N., McHarg, M. G., & Stenbaek-Nielsen, H. C. (2015). High-altitude electrical discharges associated with thunderstorms and lightning. *Journal of Atmospheric and Solar-Terrestrial Physics*, 136, 98–118. <https://doi.org/10.1016/j.jastp.2015.05.013>
- Luque, A., & Ebert, U. (2009). Emergence of sprite streamers from screening-ionization waves in the lower ionosphere. *Nature Geoscience*, 2(11), 757–760. <https://doi.org/10.1038/ngeo662>
- Luque, A., & Gordillo-Vázquez, F. J. (2012). Mesospheric electric breakdown and delayed sprite ignition caused by electron detachment. *Nature Geoscience*, 5(1), 22–25. <https://doi.org/10.1038/ngeo1314>
- Luque, A., Stenbaek-Nielsen, H. C., McHarg, M. G., & Haaland, R. K. (2016). Sprite beads and glows arising from the attachment instability in streamer channels. *Journal of Geophysical Research: Space Physics*, 121(3), 2431–2449. <https://doi.org/10.1002/2015JA022234>
- Malagón-Romero, A., Luque, A., Shuman, N. S., Miller, T. M., Ard, S. G., & Viggiano, A. A. (2024a). Associative electron detachment in sprites (hash a8ce4e6) [Software]. *GitHub*. Retrieved from <https://github.com/aluque/spritechem>
- Malagón-Romero, A., Luque, A., Shuman, N. S., Miller, T. M., Ard, S. G., & Viggiano, A. A. (2024b). Associative electron detachment in sprites (Version 2) [Dataset]. *Zenodo*. <https://doi.org/10.5281/zenodo.10219917>
- Malagón-Romero, A., Pérez-Invernón, F. J., & Gordillo-Vázquez, F. J. (2023). Chemical activity of low altitude (50 km) sprite streamers. *Journal of Geophysical Research: Atmospheres*, 128(14), e2023JD038570. <https://doi.org/10.1029/2023JD038570>
- Malagón-Romero, A., Teunissen, J., Stenbaek-Nielsen, H. C., McHarg, M. G., Ebert, U., & Luque, A. (2020). On the emergence mechanism of carrot sprites. *Geophysical Research Letters*, 47(1), e85776. <https://doi.org/10.1029/2019GL085776>

- Neubert, T., & Chanrion, O. (2013). On the electric breakdown field of the mesosphere and the influence of electron detachment. *Geophysical Research Letters*, *40*(10), 2373–2377. <https://doi.org/10.1002/grl.50433>
- Pancheshnyi, S. (2013). Effective ionization rate in nitrogen-oxygen mixtures. *Journal of Physics D*, *46*(15), 155201. <https://doi.org/10.1088/0022-3727/46/15/155201>
- Pancheshnyi, S., Biagi, S., Bordage, M. C., Hagelaar, G. J. M., Morgan, W. L., Phelps, A. V., & Pitchford, L. C. (2012). The LXCat project: Electron scattering cross sections and swarm parameters for low temperature plasma modeling. *Chemical Physics*, *398*, 148–153. <https://doi.org/10.1016/j.chemphys.2011.04.020>
- Pasko, V. P., Inan, U. S., Bell, T. F., & Taranenko, Y. N. (1997). Sprites produced by quasi-electrostatic heating and ionization in the lower ionosphere. *Journal of Geophysical Research*, *102*(A3), 4529–4562. <https://doi.org/10.1029/96JA03528>
- Passas, M., Sánchez, J., Sánchez-Blanco, E., Luque, A., & Gordillo-Vázquez, F. J. (2016). A spectrograph for the study of transient luminous events. *Applied Optics*, *55*(23), 6436. <https://doi.org/10.1364/AO.55.006436>
- Phelps, A. V., & Pitchford, L. C. (1985). Anisotropic scattering of electrons by N₂ and its effect on electron transport. *Physical Review A*, *31*(5), 2932–2949. <https://doi.org/10.1103/PhysRevA.31.2932>
- Pitchford, L. C., Alves, L. L., Bartschat, K., Biagi, S. F., Bordage, M.-C., Bray, I., et al. (2017). Lxcat: An open-access, web-based platform for data needed for modeling low temperature plasmas. *Plasma Processes and Polymers*, *14*(1–2), 1600098. <https://doi.org/10.1002/ppap.201600098>
- Rayment, S. W., & Moruzzi, J. L. (1978). Electron detachment studies between O⁻ ions and nitrogen. *International Journal of Mass Spectrometry and Ion Processes*, *26*(3), 321–326. [https://doi.org/10.1016/0020-7381\(78\)80033-3](https://doi.org/10.1016/0020-7381(78)80033-3)
- Sentman, D. D., Stenbaek-Nielsen, H. C., McHarg, M. G., & Morrill, J. S. (2008). Plasma chemistry of sprite streamers. *Journal of Geophysical Research: Atmospheres*, *113*(D11), D11112. <https://doi.org/10.1029/2007JD008941>
- Shuman, N. S., Miller, T. M., Ard, S. G., & Viggiano, A. A. (2023). Kinetics of associative detachment of O⁻ + N₂ and dissociative attachment of e⁻ + N₂O up to 1300 K. *Physical Chemistry Chemical Physics*, *25*(46), 31917–31927. ((in press-a)). <https://doi.org/10.1039/d3cp03856d>
- Soler, S., Pérez-Invernón, F. J., Gordillo-Vázquez, F. J., Luque, A., Li, D., Malagón-Romero, A., et al. (2020). Blue optical observations of narrow bipolar events by asim suggest corona streamer activity in thunderstorms. *Journal of Geophysical Research: Atmospheres*, *125*(16), e2020JD032708. <https://doi.org/10.1029/2020JD032708>
- Stenbaek-Nielsen, H. C., & McHarg, M. G. (2008). High time-resolution sprite imaging: Observations and implications. *Journal of Physics D*, *41*(23), 234009. <https://doi.org/10.1088/0022-3727/41/23/234009>
- Teunissen, J., & Ebert, U. (2017). Simulating streamer discharges in 3D with the parallel adaptive Afivo framework. *Journal of Physics D*, *50*(47), 474001. <https://doi.org/10.1088/1361-6463/aa8faf>
- Teunissen, J., & Ebert, U. (2018). Afivo: A framework for quadtree/octree AMR with shared-memory parallelization and geometric multigrid methods. *Computer Physics Communications*, *233*, 156–166. <https://doi.org/10.1016/j.cpc.2018.06.018>
- Viehland, L. A., & Mason, E. A. (1995). Transport properties of gaseous ions over a wide energy range, Part IV. *Atomic Data and Nuclear Data Tables*, *60*(1), 37–95. <https://doi.org/10.1006/adnd.1995.1004>
- Viggiano, A. A., & Morris, R. A. (1996). Rotational and vibrational energy effects on ion-molecule reactivity as studied by the VT-SIFDT technique. *Journal of Physical Chemistry*, *100*(50), 19227–19240. <https://doi.org/10.1021/jp962084x>
- Viggiano, A. A., & Williams, S. (2001). Rotational and vibrational energy effects on ion-molecule reactivity as studied by VT-SIFDT technique. In L. M. Babcock & N. G. Adams (Eds.), *Advances in gas phase ion chemistry* (Vol. 4, pp. 85–136). Elsevier. [https://doi.org/10.1016/s1071-9687\(01\)80006-x](https://doi.org/10.1016/s1071-9687(01)80006-x)